RSC Advances

ROYAL SOCIETY OF CHEMISTRY

www.rsc.org/advances

RSC Advances

ARTICLE

Flexible carbon nanofiber sponges for highly efficient and recyclable oil absorption†

Xiang Ge, [a] Wei Yang, [a] Jitong Wang, [a] Donghui Long, *[a] Licheng Ling, [a] and Wenming Qiao, *[ab]

Received 00th January 20xx,
Accepted 00th January 20xx

DOI: 10.1039/x0xx00000x

www.rsc.org/

Carbon nanofiber (CNF) sponges have been prepared though a facile chemical vapor deposition method using C_2H_4 as carbon source and Ni-Cu alloy as catalyst. The as-prepared CNF sponges are composed of three-dimensional (3D) network with thick CNFs as the reinforcing rods and thin CNFs as the binding wires that hold CNFs entangled together. Such CNF sponges exhibit controllable bulk density (0.02 ~ 0.14 g·cm^{-3}) and high porosity (92% ~ 98%) through changing catalyst amount. The CNF sponges display admirable mechanical flexibility with large compressive strain (> 90%). The CNF sponges also exhibit super hydrophobicity (contact angle > 153°) and super oleophilicity. The absorption capacities of the CNF sponges for oils can achieve 22-75 times their own weight and can even be controlled by altering their density or porosity. Furthermore, the CNF sponges demonstrate outstanding recyclability by mechanically squeezing. The present work suggests the CNF sponges a widespread potential for applications in the topics regarding envrionment protection.

1. Introduction

Catalytically grown carbon nanofibers (CNFs) are recognized as a unique fiber form of carbon nanostructures with graphene layers arranged as stacked cones, cups or plates [1-3]. They could be grown via chemical vapor deposition (CVD) using carbon feedstock over metal nanoparticles at high temperature, which is almost same to the synthesis of carbon nanotubes (CNTs) [4, 5]. However, they are different in geometry from concentric and hollow CNTs, as they can be distinguished by their stacked graphitic structures [2, 4, 5]. Such a unique structure renders them to have more active edge planes on the surface of nanofibers [6, 7], thereby making them useful as supporting materials for catalysts [8, 9], reinforcing fillers in polymeric composites [10, 11], and electrode materials for energy storage device [12, 13]. In addition, the light-weight and large surface area of CNFs make them promising candidates for environmental applications such as adsorption, filtration and separation [14-17].

However, CNFs are generally synthesized in the form of nanoscopic and fluffy powder, making their handling and large-scale application difficult [8, 9]. For example in catalysis field, especially in fixed-bed, their small size increases detrimental pressure drops along the catalyst beds even causing the blocking risk [8, 9]. One promising way to address the above problems is to assemble CNFs into 3D macroscopic monoliths such as sponges, foams or sponges [14-17]. The monoliths are a kind of 3D assembly with open and hierarchical pores and interconnected networks [18]. The 3D assembly based on silica [18], carbon [19], metal oxides [20], CNTs [21] and polymer-based CNFs [14, 17] have been fabricated and studied extensively for years, but catalytically grown 3D CNF-based monoliths are a relatively new form. The unique structure of the CNF monoliths should facilitate the exposure and connection of nearly all CNFs, thus providing possible opportunities for releasing the potential of CNFs and creating high-performance materials.

To date, several approaches have been developed to fabricate CNF-like monoliths, including CNF synthesized by hydrothermal treatment [15, 16] and polymer-based aerogels (bacterial cellulose,) pyrolyzed in an inert atmosphere [14, 17]. These 3D structures demonstrate potential applications in oil sorbents. Although these works showed the possibility to integrate individual CNF into macro-level monolith, the precise control of density and porosity of macroscopic CNF monoliths is still a challenge. Moreover, direct growth of CNF monoliths through CVD is rarely reported.

Herein, we demonstrate a facile CVD method to directly synthesize a sponge-like CNF monolith consisting of interconnected CNF skeletons. The key to this synthesis relies on the unique Ni-Cu alloy catalyst, which allows the one-step growth of octopus-like CNFs that self-assemble into a 3D entangled network. The obtained CNF sponges show controllable density and porosity, excellent mechanical flexibility, super hydrophobicity and super oleophilicity. When used as sorbent materials, the CNF sponges could absorb a wide range of oils with high absorption capacity and good recyclability. The present work provides a feasible way to

[a] State Key Laboratory of Chemical Engineering, East China University of Science and Technology, Shanghai 200237, China. E-mail: longdh@mail.ecust.edu.cn; Fax: +86 021 64252914; Tel: +86 021 64252924
[b] National Engineering Research Center of Ultrafine Powder, Shanghai 200231, China E-mail: qiaowm@ecust.edu.cn; Fax: +86 021 64252914; Tel: +86 021 64253730

†Electronic Supplementary Information (ESI) available. See DOI: 10.1039/x0xx00000x

prepare macroscopic 3D CNF sponges in a CVD system, which offers a great opportunity to develop high-performance carbon nanomaterials and explore applications in various fields.

2. Experimental section

2.1 Synthesis of CNF sponges

The non-supported Ni-Cu catalysts with different Ni/Cu mass ratios were prepared through the co-precipitation of copper and nickel carbonates from the corresponding nitrate solution using ammonium bicarbonate as co-precipitation agent, according to the reference [22]. The obtained Ni-Cu carbonates were calcined into oxides at 400 ^{o}C for 6 h. Then the oxides were reduced at 500 ^{o}C for 20 h under H_2/He (1/9, vol./vol.) atmosphere to obtain the Ni-Cu alloy catalysts (Figure S1). The reduced Ni-Cu catalyst was ground into size around tens of micrometers and stored for use. The Ni-Cu catalysts are indexed as pure Ni, Ni-Cu 8/2, Ni-Cu 7/3 and Ni-Cu 5/5, where the 8/2, 7/3 and 5/5 represent the mass ratio of the Ni-Cu catalysts.

CNF sponges were synthesized though CVD using C_2H_4 and Ni-Cu alloy as carbon source and catalyst, respectively. Catalysts were placed in a cylindrical quartz mold (Φ 25×50 mm) which was then placed in the center of CVD furnace. Before introduction of carbon feedstock, the Ni-Cu alloy catalyst was further reduced by a H_2/He (1/4, vol./vol.) mixture for 2 h at 580 ^{o}C. Then the C_2H_4/H2 mixture (4/1, vol./vol.) was introduced and held at 580 ^{o}C for 1 h to grow the CNFs. After cooling, the CNF cylinder was removed from the quartz mold.

2.2 Oil absorption of CNF aerogels

Different organics, such as hexane (0.66 g·cm^{-3}), ethanol (0.79 g·cm^{-3}), paraffin liquid (0.85 g·cm^{-3}), engine oil (0.89 g·cm^{-3}), vegetable oil (0.90 g·cm^{-3}), ethylene glycol (1.13 g·cm^{-3}), chloroform (1.50 g·cm^{-3}) and carbon tetrachloride (1.59 g·cm^{-3}), were used to test oil absorption capacity of CNF sponges. Pristine CNF cylinders were cut into small discs with the thickness of 1 cm for oil adsorption. Typically, the CNF discs were immersed into the oils for 5 minutes and then picked up with sharp needle tweezers. After the removal of the redundant oil on the surface, the CNF sponge was immediately placed onto a weigh paper to be measured on the mass balance. The weight measurements were done quickly to avoid evaporation of absorbed oils. The oil absorption capacity was calculated by the weight difference before and after the immersion. The absorption was very fast and typically reached saturation within 2 minutes by immersing the cylinders into the liquid, see Figure S2.

2.3 Characterization

Morphologies of the CNF sponges were observed under scanning electron microscope (SEM; Nova Nano 450) and transmission electron microscope (TEM; JEM-2100F, JEOL).

X-ray diffraction (XRD) was performed on a Rigaku D/Max2550VB/PC (Rigaku, Cu Ka radiation). Raman spectra were performed on a Raman microscope (iuvia refl) with an excitation wavelength of 514.5 nm.

X-ray photoelectron spectroscopy (XPS) experiments were carried out on a PHI-5000C ESCA system (Perkin Elmer) with Al Ka radiation (hm = 1486.6 eV). The base pressure of the analyzer chamber was about 5×10^{-8} Pa. Binding energies were calibrated by using the containment carbon (C 1s=284.6 eV).

The hydrophobicity and oleophilicity properties were evaluated through contact angle tests, which were performed by the CAST2.0 contact angle analysis system at room temperature.

Compression test was performed on the Transces II T2002 universal testing machine, and samples with a size of 15×15×15 mm were tested in displacement control at a rate of 1 mm/s.

The bulk density of as-grown CNF sponges was determined by measuring the mass of a fixed volume. The surface area and pore size distribution were determined by N_2 adsorption/desorption isotherms using a Quadrasorb SI analyzer.

3. Results and discussion

3.1. Synthesis of CNF aerogels

CNF sponges were directly synthesized in a quartz mold through CVD method using C_2H_4 as carbon source and Ni-Cu alloy as catalyst at a relatively low temperature of 580 ^{o}C. The total synthesis is schematically illustrated in Figure 1a. The key to the synthesis is the Ni-Cu catalyst, which led to the growth of branched CNFs that entangles together into randomly interconnected CNF network. As growth time prolongs, the entangled CNFs gradually fill the quartz mold, and finally form the aerogel-like CNF cylinder (Φ 25×50 mm, Figure 1b).

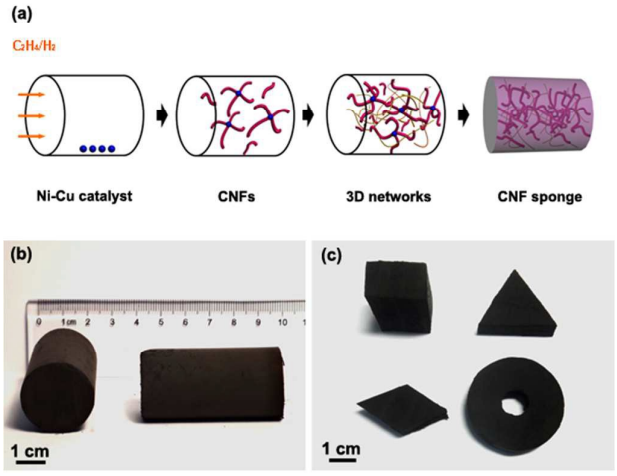

Figure 1 Formation schematic and macroscopic morphologies of CNF sponges. (a) Formation schematic of CNF sponges, (b) Macroscopic morphology of cylindrical CNF sponges, (c) CNF sponges with different macroscopic shapes.

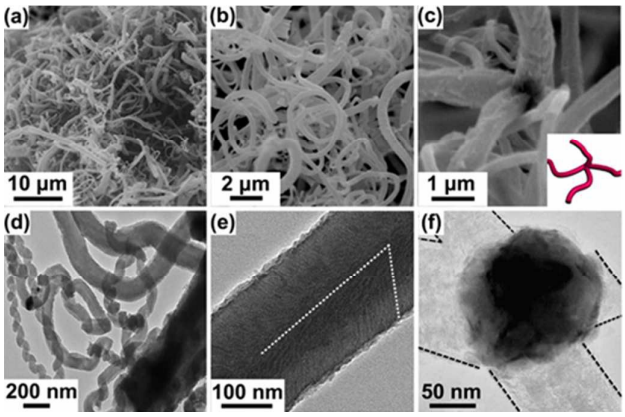

Figure 2 SEM (a-c) and TEM (d-f) images of CNF sponges. (a) 3D interconnected networks entangled by CNFs, (b) SEM closeup of CNF entanglement, (c) SEM image of branched CNFs grown from one single catalyst particle, (d) TEM closeup of CNF entanglement, (e) TEM image of a typical herringbone type CNF oriented at an angle 60° with respect to the fiber axis, (f) TEM image of branched CNFs grown from one single catalyst particle.

Here, the CNF sponges are obtained using a simple CVD system, thus it is easily scaled up by using a large mold with a large reactive chamber. In addition, the CNFs sponges can also be converted to other types of 3D shape by using suitable molds (shape and size) or by post shaping treatments as shown in Figure 1c.

SEM images of typical CNF sponges are shown in Figures 2a and 2b, which show a porous and interconnected 3D network. The diameters of the CNFs are not uniform with a range of tens to hundreds of nanometers. More typically, the thick CNFs serve as the reinforcing rods while the thin coiled-coil CNFs serve as the binding wires that hold the CNFs together. This feature should allow the CNF sponges to bear compression or strain to a certain degree. TEM images reveal that the CNFs are of the herringbone type oriented at an angle 60° with respect to the fiber axis. It is found that some CNFs grow from a single catalyst particle (Figures 2c and 2f), leading to this special octopus-like branch structure, being similar to the results reported by Pham-Huu et al [23] and Tim et al [24]. The existence of these branched CNFs should further enhance the entanglement of the fibers, which finally benefits the construction of 3D networks. No remarkable differences were observed in their morphology from top surface to side-wall and to central region (Figure S3), indicating the uniformity of the sponge.

The Ni-Cu alloy catalyst was reported to effectively grow the herringbone CNFs [2], however, only Ni-Cu with a narrow range of Cu content (20 ~ 30 wt.%) can grow the CNF sponges in this work (Figures S4b and S4c). For the cases where pure nickel catalyst or alloy catalyst with high Cu content (~50 wt.%) are used, only CNF powders could be obtained from each catalyst. SEM images indicate that the CNFs produced from pure Ni catalyst consist of short and thick CNFs, while the CNFs from high-Cu-content alloy are composed of uniform thin CNFs, both of which lack the reinforcing rod-binding wire structure (Figures S4a and S4d). In addition, the CNF yields of these catalysts are significantly lower than that of Ni-Cu (20 ~ 30% Cu) catalyst at the same growth conditions (Figure S5). These results suggest the unique Ni-Cu catalyst is the key to form 3D interconnected CNF networks.

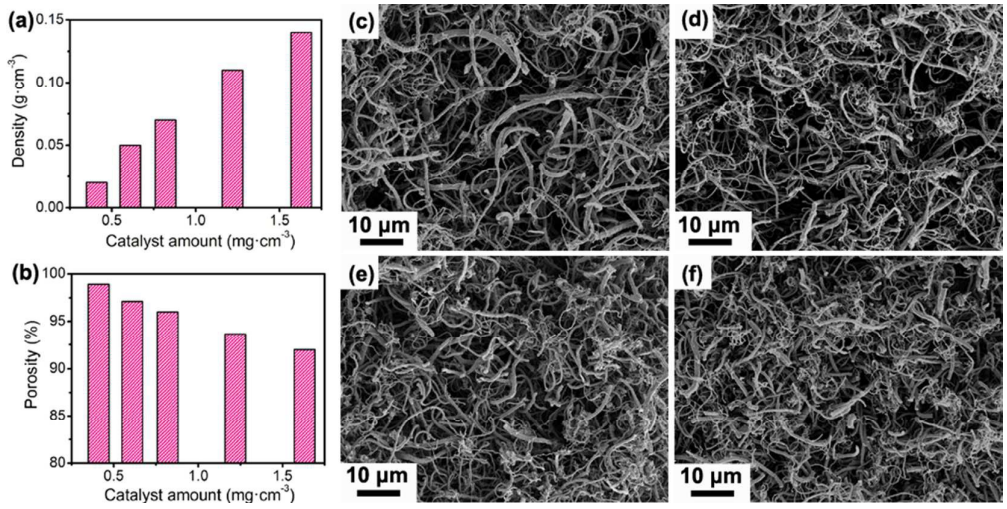

Figure 3 Effect of catalyst amount on the density, porosity and microscopic morphology of CNF sponges. (a) Variation of CNF sponges density with catalyst amount, (b) Variation of CNF sponge porosity with catalyst amount, (c)-(f) Microscopic morphologies of CNF sponges synthesized with different catalyst amounts: (c) 0.41 mg·cm^{-3}, (d) 0.61 mg·cm^{-3}, (e) 0.82 mg·cm^{-3}, (f) 1.22 mg·cm^{-3}.

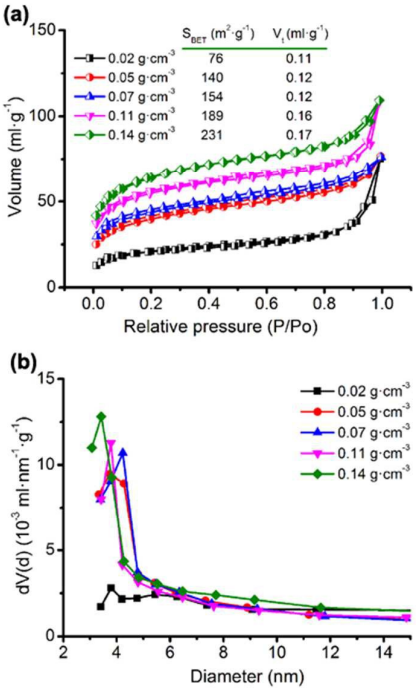

Figure 4 Adsorption/desorption isotherms (a) and pore size distribution (b) of CNF sponges.

The growth of CNF sponges is very feasible, allowing their bulk density and porosity easily controlled by changing the catalyst amount in the mold. In general, increasing the catalyst amount leads to the increase of the bulk density and the decrease of porosity while preserve their cylinder shape. As shown in Figure 3a, the density shows almost linear change, ranging from 0.02 ~ 0.14 g·cm^{-3} by changing catalyst amount. It is worth to mention that CNF sponges have the lowest density of 0.02 g·cm^{-3}, which is comparable to the aligned CNT arrays (0.01 g·cm^{-3}) [25] and 3D CNT solids (0.01 ~ 0.025 g·cm^{-3}) [26]. SEM observations demonstrate that these sponges with different densities exhibit almost similar entangled morphology regardless of the spatial compactness (Figures 3c-3e).

The N_2 adsorption/desorption was preformed to characterize the BET surface areas and pore volume of the samples (Figure 4). Generally, the materials exhibit typical type-IV isotherms with H1 and H2 hysteresis loops, and give a surface area range of 75 to 230 $m^2 \cdot g^{-1}$ (Figure 4a), depending on the density of the CNF sponges. The pore size exhibits a narrow pore size distribution of 2 to 5 nm (Figure 4b), which is normally formed by the defects on the nanofibers' surface. It should be noted that the CNF sponges are consisted of branched CNFs that entangles together into randomly interconnected network. The porosity of CNF sponges is therefore on a micrometer scale that cannot be detected by N_2 adsorption. The porosity is estimated to be 92-99% (Figure 3b) based on the calculations using a single CNF density of 1.75 g·cm-3 according to the reference [27].

The XPS spectra of the CNF sponge (density: 0.02 g·cm^{-3}) shows typical asymmetric peaks in the C 1s region (Figure S6). The atomic concentrations are 98.96% and 1.04% for C 1s and O 1s, respectively. Since the CNFs are prepared by oxygen-free CVD process, the trace oxygen atoms present on the CNF surface may be issued from surface residue or contaminants. Therefore, CNF sponges possess an inert, hydrophobic nature that is favor for oil adsorption.

CNF sponges show a prominent reflexion at ca. 26° and a weak peak at ca. 43° assigned to graphitic carbon (planes 002 and 100, respectively) in XRD pattern (Figure S7). No significant changes in reflexions assigned to graphitic carbon are observed among the CNF sponges.

CNF sponges exhibit two bands at around 1590 cm^{-1} and 1344 cm^{-1} in Ranman spectra (Figure S8), corresponding to the high crystalline graphite vibration in the tangential stretching mode (graphitic lattice mode E2g) and the disorder induced phonon mode, which originates from the mode of boundaries in Brillouin zone, respectively [29]. There is very little change in Raman spectra for CNF sponges with different densities.

3.2 Mechanical properties of CNF sponges

The as-synthesized CNF sponges display excellent structural flexibility which was rarely observed in other high-porosity materials such as silica sponges and aligned CNT arrays. Here we evaluated the structural flexibility by taking the sponge with bulk density of 0.02 g·cm^{-3} as an example. As shown in Figure 5a, the sponge recovers to nearly original shape after the removal of manual compression. No crack is observed from the exterior after the severe compression. In addition, an sponges with discoid shape can be bent without breakage, and then it still recovers to the original shape (Figure 5b). The structural flexibility under large deformation should be attributed to the reinforcing rod-binding wire CNFs networks in a 3D isotropic configuration, which can prevent the sliding or splitting between CNF sponges along any direction.

The mechanical properties of the material were further studied by uniaxial compression test. As shown in Figure 5c, all of the stress-strain curves substantially hyperbolic type without obvious yield points. The loading process shows three distinct regions [30, 31], including the elastic region during which the stress increases linearly with the strain, the plateau region from which most of the absorbed energy dissipates, and the densification region marked by the rapid increase of stress due to the continuously decreasing porosity. It is worth noting that the strain-stress curves of the CNF sponge with a density of 0.02 g·cm^{-3} exhibit broad linear-elastic regions, up to 65% strain, much higher than that of most CNT aerogels [21, 32, 33] and graphene aerogels or sponges[34-36]. The modulus of elasticity monotonically increases with increasing CNF sponge density (Figure 5d), which means the elasticity decreases while the stiffness increases.

Repeated compressions lead to plastic deformation during the loading process and rebound degree after release. The sponge with a density of 0.02 g·cm-3 can maintain most of its original compressive stress in every cycle, even compressed for 10 times with a little degradation of mechanical strength (Figure 5e). Rebound degree is measured to be ca. 98.5% after compression at 65% strain for 10 cycles (Figure 5f), indicating very little plastic deformation in the repeated test. The excellent shape and volume recovery of the CNF sponge is definitely due to the unique interconnected 3D CNF networks

which can sustain large deformation and recover back to the original shape.

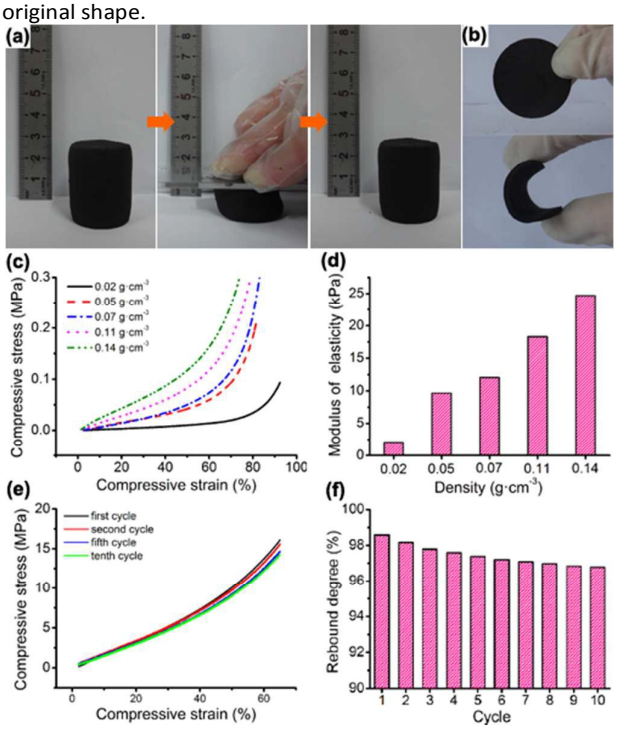

Figure 5 Mechanical properties of the CNF sponges. (a) A sponge recovered to nearly original shape after manual compression to large strain (> 50%). (b) A discoid sponge bent to a large degree. (c) Compressive stress-strain curve of CNF sponge with different densities. (d) Variation of modulus of elasticity with respect to density. (e) Cyclic compressive stress-strain curves at maximum strain of 65% (sample density: 0.02 g·cm-3). (f) Rebound degree in cyclic test at the maximum strain of 65% (sample density: 0.02 g·cm-3).

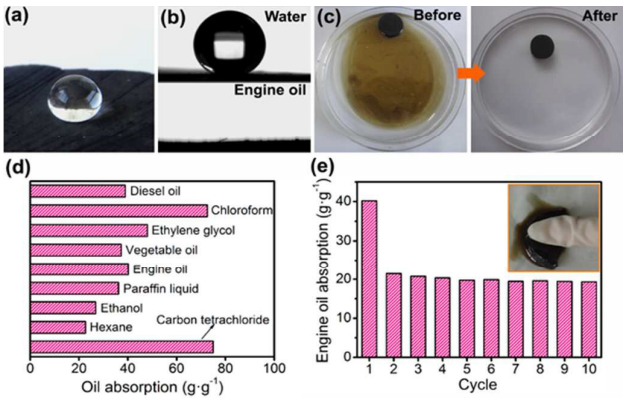

Figure 6. Oil absorption of the CNF sponges (sample density: 0.02 g·cm-3). (a) Snapshot of a water drop with a 2 mm diameter resting on the sponge surface. (b) The sponge has a water contact angle of ca. 153o and an oil contact angle of 0o (2 μL droplet). (c) Demonstration using a piece of CNF sponge to clean up used engine oil floating on water. (d) Absorption capacity of CNF sponges for common oils. (e) Recycle of the CNF sponge in oil absorption by squeezing.

3.3 Oil absorption of CNF sponges

Apart from the excellent structure flexibility, the as-synthesized CNF sponges exhibit super hydrophobicity and outstanding oleophilicity. Also taking the sample with a density of 0.02 g·cm^{-3} for example, a spherical water drop with a 2 mm diameter can remain on the hydrophobic surface without being absorbed (Figure 6a). The water contact angle measurement further shows the sponge has a contact angle ca. 153^{o} with a 2 μL water droplet (Figure 6b). In contrast to super hydrophobicity to water, the CNF sponge shows excellent oleophilic property. When an engine oil droplet drips on the surface of the CNF sponge, it is absorbed immediately and a contact angle of ca. 0^{o} is observed (Figure 6b). Therefore, the CNF sponge exhibits both super hydrophobicity and super oleophilicity, which is crucial for selective uptake of spilled oils in water.

Owing to its low density, high porosity, excellent structure flexibility, super hydrophobicity and oleophilicity, the as-synthesized CNF sponge should be an ideal candidate for the absorption of oil pollutants. In Figure 6c, the CNF aerogel can completely absorb engine oil from the water surface. The absorption process proceeds rapidly and the oil layer immediately shrinks and finally disappears completely in a few minutes. Owing to its light weight and super hydrophobicity, the sponge is always floating on the water during the absorption process. No water in the saturated CNF sponge can be found, indicating extremely high selective absorption for the oil. Therefore, the CNF sponge shows great potential for the facile removal of environmental oil contamination from water.

To further demonstrate the absorption ability of the CNF sponge, we investigated its absorption capacities for a series of common oils. As shown in Figure 6d, the CNF sponge shows a high absorption capacity for all the oils. In general, the absorption capacities range from 22 to 75 g·g^{-1}. The oils are mainly stored in the interconnected pores inside the CNF sponge, so the absorption capacity is related not only to the surface characteristics of the sponge, but also to the densities of oils [15].

Although the oil absorption performance of as-prepared CNF sponges is “slightly” common compared with other reported materials, there are some differences in oil absorption. As shown in Table 1, the absorption capacities of CNF sponges are superior to many materials, such as activated carbon [37] and zeolite [38]. They are comparable to that of magnetic CNT sponge [39], graphene sponge [40], spongy graphene [41], carbon soot sponge [42] and graphene-CNT aerogel [43], but lower than that of CNT solid [26], hydrothermal CNF aerogel [15], CNT sponge [33] and ultra-flyweight carbon aerogel [44]. However, compared with the fabrication of these materials, the CNF sponges only requires one-step facile CVD at a relatively low temperature of 580 ^{o}C, even without any pre-treatment or post-treatment, which is much more facile on a large scale than that of these absorbent counterparts (Table 1).

Table 1 Comparison of various oil absorption materials

Materials	Absorption capacity ($g \cdot g^{-1}$)	Fabrication	Recyclability	Refs
CNF sponges	22-75	One-step CVD at 580 °C	Yes	In this work
Activated carbon	< 1	--	--	37
Zeolite	5	--	--	38
Magnetic CNT sponge	49-56	CVD at 860 °C	Yes	39
CNT sponge	80-180	CVD at 860 °C	--	33
Graphene sponge	54-65	Dip-coating process	Yes	40
Spongy graphene	20-86	Hydrothermal synthesis with multi-steps: Hummer's method, hydrothermal treatment and freeze drying	Yes	41
Hydrothermal CNF aerogel	5-140	Hydrothermal synthesis with multi-steps: template preparation, hydrothermal treatment, and freeze drying	Yes	15
CNT solid	25-120	CVD at 860 °C with boron-doped process	Yes	26
Carbon soot sponge	20-80	Multi-steps including combustion flame process and dip-coating	--	42
Graphene-CNT aerogel	28-35	Hybrid of both CVD and hydrothermal synthesis	--	43
Ultra-Flyweight carbon aerogel	215-743	"sol-cryo" method including freeze-drying, reduction in hydrazine vapor	Yes	44

The recyclability of the oil absorption materials plays an important role for practical oil absorption applications [34-36]. The recycling potential of CNF sponge is evaluated through a simple squeezing by taking engine oil as an example. As shown in Figure 6e, the saturated absorption capacity rapidly decreases to 22 $g \cdot g^{-1}$ (more than half of the original absorption capacity) from the second cycle after squeezing, since the absorbed engine oil cannot be completely extruded by applying a hand stress. The result indicates that about 18 $g \cdot g^{-1}$ of engine oil remains in the CNF sponge after squeezing. After that, the saturation absorption capacity remains steady at about 20 $g \cdot g^{-1}$ in the subsequent cycles, indicating that the absorption effectiveness of the CNF sponge does not remarkedly change in subsequent cycles.

Additionally, the absorption capacities of the CNF sponges can be controlled by altering their density or porosity. As shown in Figure 7, the sponges with lower density (higher porosity) possess larger absorption capacity. Meanwhile, the CNF sponges have higher absorption capacity for higher-density oils (e.g., carbon tetrachloride).

4 Conclusions

In summary, CNF sponges were synthesized through facile CVD using C_2H_4 as carbon source and Ni-Cu alloy as catalyst. The sponges are composed of 3D herringbone CNF networks with the thick CNFs serving as the reinforcing rods and the thin CNFs serving as the binding wires that hold the CNFs together. This feature should allow the CNF sponges to bear compress or strain to a certain degree. In addition, CNF sponges exhibit a variety of superior properties, including low density, high porosity, super hydrophobicity and excellent oleophilicity. As an oil absorbent, the sponges exhibit high absorption capacity ranging from 22 to 75 $g \cdot g^{-1}$ for a series of oils. Significantly, the CNF sponges display outstanding absorption recyclability by mechanically squeezing. Due to these peculiar properties, the CNF sponges are demonstrated to be a new kind of excellent reusable sorbent materials for oil absorption.

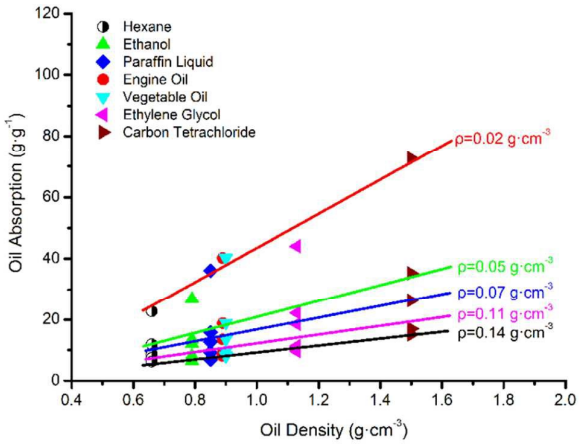

Figure 7 Oil absorption capacity for common oils measured with CNF sponges with different densities.

Acknowledgements

This work was partly supported by MOST (2014CB239702), National Science Foundation of China (20977028, 51172071, 51272077), Program of Shanghai Subject Chief Scientist (B type, No 13XD1424900), and Fundamental Research Funds for the Central Universities.

Notes and references

1 N. M. Rodriguez, A. Chambers and R. T. K. Baker, *Langmuir*, 1995, **11**, 3862-3866.
2 S. H. Yoon, S. Lim, S. h. Hong, W. Qiao, D. D. Whitehurst, I. Mochida, B. An and K. Yokogawa, *Carbon*, 2005, **43**, 1828-1838.
3 D. Long, J. Hong, W. Li, J. Miyawaki, L. Ling, I. Mochida, S. Yoon and J. Jang, *ACS Nano*, 2011, **5**, 6254-6261.
4 H. Wang and J. J. Moore, *Carbon*, 2012, **50**, 1235-1242.
5 D. Long, W. Li, J. Miyawaki, W. Qiao, L. Ling, I. Mochida and S. H. Yoon, *Chem. Mater.*, 2011, **23**, 4141-4148.
6 K. P. De Jong and J. W. Geus, *Catal. Rev.*, 2000, **42**, 481-510.
7 M. Endo, Y. A. Kim, M. Ezaka, K. Osada, T. Yanagisawa, T. Hayashi, M. Terrones and M. S. Dresselhaus, *Nano Lett.*, 2003, **3**, 723-726.
8 M. K. van der Lee, A. J. van Dillen, J. W. Geus, K. P. de Jong and J. H. Bitter, *Carbon*, 2006, **44**, 629-637.
9 R. Vieira, C. Pham-Huu, N. Keller and M. J. Ledoux, *Chem. Commun.*, 2002, 954-955.
10 M. H. Al-Saleh and U. Sundararaj, *Carbon*, 2009, **47**, 2-22.
11 Y. Yang, M. C. Gupta, K. L. Dudley and R. W. Lawrence, *Adv. Mater.*, 2005, **17**, 1999-2003.
12 Z. Fan, J. Yan, T. Wei, L. Zhi, G. Ning, T. Li and F. Wei, *Adv. Funct. Mater.*, 2011, **21**, 2366-2375.
13 Y. Yu, L. Gu, C. Wang, A. Dhanabalan, P. A. van Aken and J. Maier, *Angew. Chem. Int. Ed.*, 2009, **48**, 6485-6489.
14 H. Bi, Z. Yin, X. Cao, X. Xie, C. Tan, X. Huang, B. Chen, F. Chen, Q. Yang, X. Bu, X. Lu, L. Sun and H. Zhang, *Adv. Mater.*, 2013, **25**, 5916-5921.
15 Z. Y. Wu, C. Li, H. W. Liang, Y. N. Zhang, X. Wang, J. F. Chen and S. H. Yu, *Sci. Rep.*, 2014, **4**, 4079.
16 H. W. Liang, Q. F. Guan, L. F. Chen, Z. Zhu, W. J. Zhang and S. H. Yu, *Angew. Chem. Int. Ed.*, 2012, **51**, 5101-5105.
17 Z. Y. Wu, C. Li, H. W. Liang, J. F. Chen and S. H. Yu, *Angew. Chem. Int. Ed.*, 2013, **52**, 2925-2929.
18 D. W. Schaefer and K. D. Keefer, *Phys. Rev. Lett.*, 1986, **56**, 2199.
19 D. Long, Q. Chen, W. Qiao, L. Zhan, X. Liang and L. Ling, *Chem. Commun.*, 2009, 3898-3900.
20 D. J. Suh and T. J. Park, *Chem. Mater.*, 1996, **8**, 509-513.
21 M. B. Bryning, D. E. Milkie, M. F. Islam, L. A. Hough, J. M. Kikkawa and A. G. Yodh, *Adv. Mater.*, 2007, **19**, 661-664.
22 A. Tanaka, S. H. Yoon and I. Mochida, *Carbon*, 2004, **42**, 1291-1298.
23 C. Pham-Huu, R. Vieira, B. Louis, A. Carvalho, J. Amadou, T. Dintzer and M. J. Ledoux, *J. Catal.*, 2006, **240**, 194-202.
24 J. M. Ting and R. M. Liu, *Carbon*, 2003, **41**, 601-603.
25 M. Yu, H. H. Funke, J. L. Falconer and R. D. Noble, *Nano Lett.*, 2008, **9**, 225-229.
26 D. P. Hashim, N. T. Narayanan, J. M. Romo-Herrera, D. A. Cullen, M. G. Hahm, P. Lezzi, J. R. Suttle, D. Kelkhoff, E. Munoz-Sandoval and S. Ganguli, *Sci. Rep.*, 2012, **2**.
27 N. M. Rodriguez, *J. Mater. Res.*, 1993, **8**, 3233-3250.
28 J. H. Zhou, Z. J. Sui, J. Zhu, P. Li, D. Chen, Y. C. Dai, W. K. Yuan. *Carbon,* 2007, **45**, 785-796.
29 A.G. Souza Filho, A. Jorio, G.G. Samsonidze, G. Dresselhaus, R. Saito and M.S. Dresselhaus, *Nanotechnology,* 2003, **14**, 1130-1139.
30 H. W. Liang, Q. F. Guan, L. F. Chen, Z. Zhu, W. J. Zhang and S. H. Yu, *Angew. Chem. Int. Ed.*, 2012, **51**, 5101-5105.
31 A. Cao, P. L. Dickrell, W. G. Sawyer, M. N. Ghasemi-Nejhad and P. M. Ajayan, *Science*, 2005, **310**, 1307-1310.
32 J. Zou, J. Liu, A. S. Karakoti, A. Kumar, D. Joung, Q. Li, S. I. Khondaker, S. Seal and L. Zhai, *Acs Nano*, 2010, **4**, 7293-7302.
33 X. Gui, J. Wei, K. Wang, A. Cao, H. Zhu, Y. Jia, Q. Shu and D. Wu, *Adv. Mater.*, 2010, **22**, 617-621.
34 L. Qiu, J. Z. Liu, S. L. Chang, Y. Wu and D. Li, *Nat. Commun.*, 2012, **3**, 1241.
35 H. Hu, Z. Zhao, W. Wan, Y. Gogotsi and J. Qiu, *Adv. Mater.*, 2013, **25**, 2219-2223.
36 E. Yoo, T. Okata, T. Akita, M. Kohyama, J. Nakamura and I. Honma, *Nano Lett.*, 2009, **9**, 2255-2259.
37 M. Lillo-Ródenas, D. Cazorla-Amorós and A. Linares-Solano, *Carbon*, 2005, **43**, 1758-1767.
38 T. Sakthivel, D. L. Reid, I. Goldstein, L. Hench and S. Seal, *Environ. Sci. Technol.*, 2013, **47**, 5843-5850.
39 X. Gui, Z. Zeng, Z. Lin, Q. Gan, R. Xiang, Y. Zhu, A. Cao and Z. Tang, *ACS Appl. Mater. Inter.*, 2013, **5**, 5845-5850.
40 D. D. Nguyen, N. H. Tai, S. B. Lee and W. S. Kuo, *Energy Environ. Sci.*, 2012, **5**, 7908-7912.
41 H. Bi, X. Xie, K. Yin, Y. Zhou, S. Wan, L. He, F. Xu, F. Banhart, L. Sun and R. S. Ruoff, *Adv. Funct. Mater.*, 2012, **22**, 4421-4425.
42 Y. Cao, Y. S. Zhou, W. Xiong, M. Wang, L. Fan, H. Rabiee-Golgir, L. Jiang, W. Hou, X. Huang, L. Jiang, J. F. Silvain and Y. F. Lu, *Appl. Mater. Inter.,* 2014, **6**, 5924-5929.
43 S. Kabiri, D. N. H. Tran, T. Altalhi and D. Losic, *Carbon,* 2014, **80**, 523-533.
44 H. Sun, Z. Xu and C. Gao, Adv. Mater., 2013, 25, 2554-2560.